International Journal for Research in Engineering Application & Management (IJREAM)
ISSN : 2454-9150 Vol-04, Issue-10, Jan 2019

Rivlin-Ericksen Fluid Effect On Mixed Convective Fluid Flow Past A Wavy Inclined Porous Plate In Presence Of Soret, Dufour, Heat Source And Thermal Radiation: A Finite Difference Technique

V. Omeshwar Reddy[1], Assiatant Professor, TKR College of Engineering and Technology, Hyderabad, Telangana State, India. omesh.reddy1110@gmail.com

S. Thiagarajan[2] , Professor, Matrusri Engineering College, Saidabad, Hyderabad, Telangana State, India. drthiagarajan@gmail.com

ABSTRACT: Present investigation involves study of thermal diffusion, diffusion thermo, thermal radiation and heat generation effects on the unsteady magnetohydrodynamic flow of electrically conducting Rivlin-Ericksen fluid flow past over an infinte vertically inclined plate through porous medium. Mathematical modeling of the problem gives rise to system of linear partial differential equations, and is solved numerically using finite difference technique. Effects of pertinent parameters on the fluid flow, heat and mass transfer characteristics have been studied graphically and the physical aspects are discussed in detail. With the help of velocity, temperature and concentration; skin friction, nusselt number and sherwood number are derived and represented through tabular form. We found an excellent agreement of the present results by comparing with the published results. It is found that Soret and Dufour parameters regulate the heat and mass transfer rate. Nonlinear thermal radiation effectively enhances the thermal boundary layer thickness.

KEYWORDS*: *Mixed Convection, Porous Medium, Soret; Dufour, Thermal radiation, Finite Difference Method.

NOMENCLATURE:

List of variables:

A	A positive constant
Q	Dimensional Heat absorption parameter
U_∞	Dimensionless free stream velocity,
S	Dimensionless Heat absorption parameter
Du	Dufour number (Diffusion thermo)
U_p	Dimensionless plate translational Velocity
U_o	Moving velocity ($m\ s^{-1}$)
K	Permeability parameter ($K\ d^{-2}$)
Re_x	Reynold's number
V_o	Suction velocity ($m\ s^{-1}$)
R	Thermal Radiation absorption parameter
M	Hartmann number
n	Dimensionless free stream frequency of oscillation (s^{-1})
$K_{\lambda w}$	Radiation absorption coefficient
Sc	Schmidt Number
Sr	Soret Number (Thermal diffusion)
Pr	Prandtl number
g	Acceleration due to Gravity, 9.81 (m/s^2)
C'_∞	Concentration at free stream ($Kg\ m^{-3}$)
C'_w	Concentration at the wall ($Kg\ m^{-3}$)
C_s	Concentration susceptibility ($m\ mole^{-1}$)
x'	Coordinate axis along the plate (m)
y'	Coordinate axis normal to the plate (m)
C'	Dimensional Fluid Concentration
T'	Dimensional Fluid temperature (K)
u'	Dimensional Velocity ($m\ s^{-1}$)
Kr	Dimensionless Chemical reaction parameter
x	Dimensionless Coordinate axis along the plate (m)
y	Dimensionless Coordinate axis normal to the plate (m)
t	Dimensionless time (s)
u	Dimensionless Velocity ($m\ s^{-1}$)
T'_∞	Fluid temperature at free stream (K)
T'_w	Fluid temperature at the wall (K)
v	Dimensionless velocity in $y'-$ direction
Gr	Grashof Number for heat transfer

 DOI : 10.18231/2454-9150.2018.1296

Gc	Grashof Number for mass transfer
B_o	Magnetic field ($tesla$)
k_T	Mean absorption coefficient
T_m	Mean fluid temperature (K)
D_m	Molecular diffusivity ($m^2\ s^{-1}$)
$e_{b\lambda}$	Plank's function ($N\ m\ s$)
P	Pressure ($N\ m^{-2}$)
Nu	Rate of heat transfer (or) Nusselt number
Sh	Sherwood number
Cf	Skin-friction Coefficient ($N\ m^{-2}$)
D	Solute mass diffusivity ($m^2\ s^{-1}$)
C_P	Specific heat at constant pressure ($J\ Kg^{-1}K$)
Greek Symbols	
β^*	Coefficient of Compositional expansion ($m^3\ Kg^{-1}$)
β	Coefficient of thermal expansion (K^{-1})
ϕ	Dimensionless concentration ($Kg\ m^{-3}$)
α	Angle of inclination ($\deg rees$)
λ	Rivlin-Ericksen fluid parameter
θ	Dimensionless Temperature away from the plate (K)
σ	Electrical conductivity, *Henry/meter*
ρ	Fluid density ($Kg\ m^{-3}$)
ν	Kinematic viscosity ($m^2\ s^{-1}$)
ε	Porosity of the porous medium $(\varepsilon < 1)$
τ'_w	Shear Stress (*Pascal*)
κ	Thermal conductivity ($W\ m^{-1}K^{-1}$)
Superscripts	
'	Dimensional Properties
Subscripts	
∞	Free stream conditions
p	Conditions at the plate
w	Conditions on the wall

I. INTRODUCTION

The role of thermal radiation on the flow and heat transfer process is of major importance in the design of many advanced energy conversion systems operating at higher temperature e.g. Nuclear power plants, gas turbines and various propulsion devices for aircraft, missiles, satellites and space vehicles. Thermal radiation within this system is usually as a result of emission by hot walls and the working fluid Seigel and Howell [1]. In the similar input, Effect of thermal radiation and soret in the presence of heat source/sink on unsteady MHD flow past a semi-infinite vertical plate was studied by Srihari and Srinivas [2]. Non-aligned MHD stagnation point flow of variable viscosity nanofluids past a stretching sheet with radiative heat was investigated by Waqar et al. [3]. They transformed the governing nonlinear partial differential equations into a set of nonlinear ordinary differential equations using similarity transformation and solved by fourth-fifth order Runge-Kutta-Tehlberg method. It was found that non-alignment of the re-attachment point on the sheet surface decreases with increase in magnetic field intensity. Makinde et al. [4] discussed the MHD variable viscosity reacting flow over a convectively heated plate in a porous medium with thermophoresis and radiative heat transfer. The system of nonlinear ordinary differential equations governing the flow is solved numerically using the Nachtsheim and Swigert shooting iteration technique together with a sixth-order Runge-Kutta iteration algorithm. Free convection effects on perfectly conducting fluid were studied by Magdy [5]. It was noticed that in both cooling and heating of the surface as Alfven velocity increases, the velocity of the flow reduces significantly. They explained that this may be due to the fact that the effect of the magnetic field corresponds to a term signifying a positive force that tends to decelerate the fluid particles. The proper understanding of radiative heat transport mechanism is quite essential for the standard quality product in industrial processes. The role of radiative heat transfer is quite phenomenal in various engineering manufacturing processes like hypersonic fights, space vehicles, gas turbines, nuclear power plants, gas cooled nuclear reactors etc. Pal and Mandal [6] has explored the impacts of radiative convection in MHD flow of nano liquid generated by a nonlinear boundary. Lin et al. [7] considered the Marangonic convection in laminar flow of copper-water nano liquid driven by thermally exponential temperature. A numerical treatment for MHD flow of Al_2O_3-water nanoparticles through thermal radiation is provided made by Sheikholeslami et al. [8]. Shehzad et al. [9] considered the effect of magnetic field and thermal radiation in laminar flow of 3D-Jeffrey nanofluid by a bidirectional moving sheet. Ibrahim et al. [10] investigated the similarity reductions for problem of radiative and magnetic field effects on free convection and mass-transfer flow past a semi-infinite verticle flat plate. Many processes in engineering areas occur at high temperature and knowledge of radiation heat transfer becomes very important for the design of the pertinent equipment [11]. S.S Ghadikolaei et al. [12] analyzed the boundary layer micropolar dusty fluid with TiO_2 nanoparticles in a porous medium under the effect of magnetic field and thermal radiation over a stretching sheet. Numerical study on heat transfer and three-dimensional magnetohydrodynamic (MHD) flow due viscous nanofluid on a bidirectional non-linear stretching sheet in the

 DOI : 10.18231/2454-9150.2018.1296

considering the viscous dissipation, thermal radiation and Joule heating effects was carried out by Mahanthesh et al. [13]. Numerical analysis magnetohydrodynamic (MHD) three-dimensional flow of nanofluids in the presence of thermal radiation and slip condition on a nonlinear stretching surface by using shooting method have been doing by Mahanthesh et al. [14]. Hossain et al. [15] studied the effect of radiation on free convection from a porous vertical plate. Srinivasacharya and Mendu [16] studied free convection in MHD micro polar fluid with radiation and chemical reaction effects. Srinivasacharya and RamReddy [17] studied natural convection heat and mass transfer in a micro polar fluid with thermal and mass stratification. Seddeek et al. [18] found effects of chemical reaction and variable viscosity on hydromagnetic mixed convection heat and mass transfer for Hiemenz flow through porous media with radiation. Ibrahim et al. [19] studied effect of the chemical reaction and radiation absorption on the unsteady MHD free convection flow past a semi-infinite vertical permeable moving plate with heat source and suction. Makinde et al. [20] investigated unsteady convection with chemical reaction and radiative heat transfer past a flat porous plate moving through a binary mixture. Radiation and Dufour effects on unsteady MHD mixed convective flow in an accelerated vertical wavy plate with varying temperature and mass diffusion discussed by Jagdish Prakash et al. [21]. Magnetohydrodynamics (MHD) has many industrial applications such as physics, chemistry and engineering, crystal growth, metal casting and liquid metal cooling blankets for fusion reactors. The convective heat transfer over a stretching surface with applied magnetic field was presented by Vajravelu et al. [22].

The present objective is to attempt a mathematical model of heat and mass transfer in Rivlin-Ericksen fluid flow over a permeable moving plate with thermal radiation in the presence of applied magnetic field, heat absorption, cross diffusion effects. The study has importance in many metallurgical processes including magma flows, polymer and food processing, and blood flow in micro-circulatory system etc. Non-dimensional variables are employed to convert the nonlinear partial differential equations into linear partial differential equations. The transformed linear partial differential equations are solved numerically using finite difference technique. Graphs for various pertinent parameters on the velocity, temperature and concentration are presented and analyzed in detail. The numerical values of Skin-friction coefficients, local Nusselt and Sherwood number coefficients are tabulated and examined. Also, a comparison of current study to the previous ones (Jagdish Prakash et al. [21]) is provided to validate our numerical solutions.

II. MATHEMATICAL FORMULATION

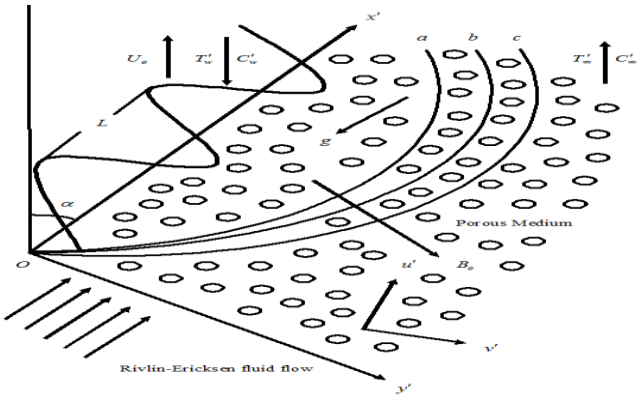

Fig. 1. The physical representation and coordinate system of the problem

a --- Momentum boundarylayer, *b* --- Thermal boundarylayer, *c* --- Concentration boundarylayer

The influence of Rivilin-Ericksen fluid on an unsteady mixed convection flow of an incompressible, viscous, electrically conducting and thermal radiating fluid past a semi-infinite vertically inclined permeable wavy plate subject to varying temperature and concentration was considered for the study. Fig. 1 represents the physical model and the coordinate system. For this investigation, we made the following assumptions:

i. In Cartesian coordinate system, let $x'-$ axis is taken to be along the plate and the $y'-$ axis normal to the plate.
ii. Since the plate is considered infinite in $x'-$ direction, hence all physical quantities will be independent of $x'-$ direction.
iii. Let the components of velocity along x' and y' axes be u' and v' which are chosen in the upward direction along the plate and normal to the plate respectively.
iv. Initially, the plate and the fluid are at the same temperature T'_∞ and the concentration C'_∞. At a time $t' > 0$, the plate temperature and concentration are raised to T'_w and C'_w respectively and are maintained constantly thereafter.
v. In the $y'-$ direction, a uniform magnetic field of magnitude B_o is maintained and in the positive $x'-$ direction, the plate moves uniformly with velocity U_o.

 DOI : 10.18231/2454-9150.2018.1296

vi. The magnetic dissipation (Joule heating of the fluid) and Hall Effect of magnetohydrodynamics are neglected.

vii. The external electric field is assumed as zero and the electric field caused by the polarization of charges is negligible.

viii. The fluid is assumed to be slightly conducting, and hence the magnetic Reynolds number is much less than unity and the induced magnetic field is negligible in comparison with the applied magnetic field.

ix. All the fluid properties are also assumed to be constant except the density variation with temperature and concentration in the body force term (Boussinesq's approximation).

x. The governing equations for this investigation are based on the balances of mass, linear momentum, energy and concentration species.

Under these assumptions, the governing boundary layer equations of the flow field are (Jagdish Prakash et al. [21]):

Equation of Continuity:

$$\frac{\partial v'}{\partial y'} = 0 \tag{1}$$

Momentum Equation:

$$\frac{\partial u'}{\partial t'} + v'\frac{\partial u'}{\partial y'} = -\frac{1}{\rho}\left(\frac{\partial p}{\partial x'}\right) + \nu\frac{\partial^2 u'}{\partial y'^2} - \left[\frac{\sigma B_0^2}{\rho}\right]u' - \left[\frac{\nu}{k'}\right]u' + g\beta(T'-T'_\infty)(\cos\alpha) + g\beta^*(C'-C'_\infty)(\cos\alpha) - \beta_1\left(\frac{\partial^3 u'}{\partial t'\partial y'^2}\right) \tag{2}$$

Energy Equation:

$$\frac{\partial T'}{\partial t'} + v'\frac{\partial T'}{\partial y'} = \frac{\kappa}{\rho C_P}\left(\frac{\partial^2 T'}{\partial y'^2}\right) - \frac{Q}{\rho C_P}(T'-T'_\infty) - \frac{1}{\rho C_P}\left(\frac{\partial q'}{\partial y'}\right) + \frac{D_m k_T}{C_s C_P}\left(\frac{\partial^2 C'}{\partial y'^2}\right) \tag{3}$$

Species Diffusion Equation:

$$\frac{\partial C'}{\partial t'} + v'\frac{\partial C'}{\partial y'} = D\left(\frac{\partial^2 C'}{\partial y'^2}\right) - K'_r(C'-C'_\infty) + \frac{D_m k_T}{T_m}\left(\frac{\partial^2 T'}{\partial y'^2}\right) \tag{4}$$

The corresponding boundary conditions of the flow are

$$\left.\begin{array}{l} t' \le 0: \ \{u' = 0, \ \ T' = T'_\infty, \ \ C' = C'_\infty \quad for \ \ all \ \ y' \\ t' > 0: \ \begin{cases} u' = U'_p, \ \ \dfrac{\partial T'}{\partial y'} = B'(T'_w - T'_\infty), \ \ \dfrac{\partial C'}{\partial y'} = B'(C'_w - C'_\infty) \ \ at \ \ y' = B'\sin\left(\dfrac{2\pi x'}{L}\right) \\ u' = U'_\infty = U_o\left(1+\varepsilon e^{n't'}\right), \ \ T' \to T'_\infty, \ \ C' \to C'_\infty \quad as \ \ y' \to \infty \end{cases} \end{array}\right\} \tag{5}$$

The suction velocity is assumed to take the following exponential form as the suction velocity at the plate surface is a function of time only:

$$v' = -V_o\left(1 + A\varepsilon e^{n't'}\right) \tag{6}$$

Where A is a real positive constant, ε and $A\varepsilon$ are less than unity and V_o is a scale of suction velocity which has a non-zero positive constant. Eq. (2) outside the boundary layer is as follows:

$$-\frac{1}{\rho}\left(\frac{\partial p}{\partial x'}\right) = \frac{dU'_\infty}{dt'} + \left[\frac{\sigma B_0^2}{\rho} + \frac{\nu}{k'}\right]U'_\infty \tag{7}$$

Where pressure p is independent of y'. The relatively low density fluid is optically thin and the radiative heat flux discussed by Cogley et al. [23] is given by:

$$\frac{\partial q'}{\partial y'} = 4(T'-T'_\infty)I \tag{8}$$

Where $I = \int_0^\infty K_{\lambda w}\left(\frac{\partial e_{b\lambda}}{\partial T'}\right)d\lambda$.

Introducing the following non-dimensional quantities:

 DOI : 10.18231/2454-9150.2018.1296

$$\left.\begin{aligned} &u=\frac{u'}{U_0},v=\frac{v'}{V_0},x=\frac{x'}{L},y=\frac{V_0y'}{\nu},U_\infty=\frac{U'_\infty}{U_o},t=\frac{V_0^2t'}{\nu},U_p=\frac{U'_p}{U_o},\theta=\frac{T'-T'_\infty}{T'_w-T'_\infty},Du=\frac{D_mk_T(C'_w-C'_\infty)}{\nu C_sC_p(T'_w-T'_\infty)},\\ &\phi=\frac{C'-C'_\infty}{C'_w-C'_\infty},n=\frac{n'\nu}{V_o^2},Sc=\frac{\nu}{D},M=\frac{\sigma\nu B_0^{\,2}}{\rho V_0^{\,2}},K=\frac{\nu^2}{V_o^2k'},Gr=\frac{g\beta\,\nu\,(T'_w-T'_\infty)}{U_oV_0^2},\ Kr=\frac{K'_r\nu}{V_o^2},B'=\frac{\nu}{V_o},\\ &Gc=\frac{g\beta^*\nu\,(C'_w-C'_\infty)}{U_oV_0^2},S=\frac{\nu Q}{\rho C_pV_0^{\,2}},R=\frac{4\nu I}{\rho C_pV_o^2},\Pr=\frac{\rho\nu C_p}{\kappa},Sr=\frac{D_mk_T(T'_w-T'_\infty)}{\nu T_m(C'_w-C'_\infty)},\lambda=\frac{\beta_1U_o^2}{\nu^2}\end{aligned}\right\} \quad (9)$$

Using Eqs. (6), (7), (8) and (9), the basic Eqs. (2)-(4) can be expressed in non-dimensional form as:

Momentum Equation:

$$\frac{\partial u}{\partial t}-\left(1+\varepsilon Ae^{nt}\right)\frac{\partial u}{\partial y}=\frac{dU_\infty}{\partial t}+\frac{\partial^2u}{\partial y^2}+N\left(U_\infty-u\right)+Gr\left(\cos\alpha\right)\theta+Gc\left(\cos\alpha\right)\phi+\lambda\left(\frac{\partial^3u}{\partial t\partial y^2}\right) \quad (10)$$

Energy Equation:

$$\left(\Pr\right)\frac{\partial\theta}{\partial t}-\left(\Pr\right)\left(1+\varepsilon Ae^{nt}\right)\frac{\partial\theta}{\partial y}=\frac{\partial^2\theta}{\partial y^2}-\left(\Pr\right)\left(R+S\right)\theta+\left(\Pr\right)\left(Du\right)\left(\frac{\partial^2\phi}{\partial y^2}\right) \quad (11)$$

Species Diffusion Equation:

$$\left(Sc\right)\frac{\partial\phi}{\partial t}-\left(Sc\right)\left(1+\varepsilon Ae^{nt}\right)\frac{\partial\phi}{\partial y}=\frac{\partial^2\phi}{\partial y^2}-\left(Kr\right)\left(Sc\right)\phi+\left(Sr\right)\left(Sc\right)\left(\frac{\partial^2\theta}{\partial y^2}\right) \quad (12)$$

And the corresponding boundary conditions are:

$$\begin{aligned} &t\le 0:\ \{u=0,\ \ \theta=0,\ \ \phi=0\ \ \ for\ \ all\ \ y\\ &t>0:\ \begin{cases} u=U_p,\ \ \dfrac{\partial\theta}{\partial y}=1,\ \ \dfrac{\partial\phi}{\partial y}=1\ \ at\ \ y=h\\ u=U_\infty=1+\varepsilon e^{nt},\ \ \theta\to 0,\ \ \phi\to 0\ \ \ as\ \ y\to\infty \end{cases}\end{aligned} \quad (13)$$

All the symbols are defined in nomenclature. The mathematical statement of the problem is now complete and represents the solutions of Eqs. (10), (11) and (12) subject to boundary conditions (13). For realistic engineering applications and the design of chemical engineering systems based on this type of boundary layer flow, the Skin-friction, Nusselt number (Rate of heat transfer) and Sherwood number (Rate of mass transfer) are important physical parameters. The non-dimensional form of the Skin-friction at the plate is given by

$$C_f=\frac{\tau'_w}{\rho U_oV_o}=\left(\frac{\partial u}{\partial y}\right)_{y=0} \quad (14)$$

The rate of heat transfer coefficient, which in the non-dimensional form in terms of the Nusselt number is given by

$$Nu=-x'\frac{\left(\dfrac{\partial T'}{\partial y'}\right)_{y'=0}}{T'_w-T'_\infty}\ \Rightarrow Nu\,\mathrm{Re}_x^{-1}=-\left(\frac{\partial\theta}{\partial y}\right)_{y=0} \quad (15)$$

The non-dimensional form rate of mass transfer coefficient in terms of the Sherwood number, is given by

$$Sh=-x'\frac{\left(\dfrac{\partial C'}{\partial y'}\right)_{y'=0}}{C'_w-C'_\infty}\ \Rightarrow Sh\,\mathrm{Re}_x^{-1}=-\left(\frac{\partial\phi}{\partial y}\right)_{y=0}\qquad \text{Where } \mathrm{Re}_x=\frac{U_ox'}{\nu} \quad (16)$$

III. NUMERICAL SOLUTIONS BY FINITE DIFFERENCE METHOD:

The non-linear momentum, energy and concentration equations given in equations (10), (11) and (12) are solved under the appropriate initial and boundary conditions (13) by the implicit finite difference method. The transport equations (10), (11) and (12) at the grid point (*i*, *j*) are expressed in difference form using Taylor's expansion.

 DOI : 10.18231/2454-9150.2018.1296

$$\left(\frac{u_i^{j+1}-u_i^j}{\Delta t}\right)-\left(1+\varepsilon Ae^{nt}\right)\left(\frac{u_{i+1}^j-u_i^j}{\Delta y}\right)=\frac{dU_\infty}{dt}+\left(\frac{u_{i+1}^j-2u_i^j+u_{i-1}^j}{(\Delta y)^2}\right)+(Gr)(\cos\alpha)\theta_i^j+$$

$$(Gc)(\cos\alpha)\phi_i^j+N\left(U_\infty-u_i^j\right)-\lambda\left[\begin{array}{l}\left(\frac{u_{i+1}^{j+1}-2u_i^{j+1}+u_{i-1}^{j+1}-u_{i+1}^j+2u_i^j-u_{i-1}^j}{\Delta t(\Delta y)^2}\right)\\-\left(1+\varepsilon Ae^{nt}\right)\left(\frac{u_{i+1}^j-3u_{i-1}^j+3u_{i-2}^j-u_{i-3}^j}{(\Delta y)^3}\right)\end{array}\right] \quad (17)$$

$$(\Pr)\left(\frac{\theta_i^{j+1}-\theta_i^j}{\Delta t}\right)-\left(1+\varepsilon Ae^{nt}\right)(\Pr)\left(\frac{\theta_{i+1}^j-\theta_i^j}{\Delta y}\right)=\left(\frac{\theta_{i+1}^j-2\theta_i^j+\theta_{i-1}^j}{(\Delta y)^2}\right)-(\Pr)(R+S)\theta_i^j$$

$$+(\Pr)(Du)\left(\frac{\phi_{i+1}^j-2\phi_i^j+\phi_{i-1}^j}{(\Delta y)^2}\right) \quad (18)$$

$$(Sc)\left(\frac{\phi_i^{j+1}-\phi_i^j}{\Delta t}\right)-\left(1+\varepsilon Ae^{nt}\right)(Sc)\left(\frac{\phi_{i+1}^j-\phi_i^j}{\Delta y}\right)=\left(\frac{\phi_{i+1}^j-2\phi_i^j+\phi_{i-1}^j}{(\Delta y)^2}\right)$$

$$-(Kr)(Sc)\phi_i^j+(Sc)(Sr)\left(\frac{\theta_{i+1}^j-2\theta_i^j+\theta_{i-1}^j}{(\Delta y)^2}\right) \quad (19)$$

Where the indices i and j refer to y and t respectively. The initial and boundary conditions (13) yield

$$\left.\begin{array}{l}u_i^0=0,\ \theta_i^0=0,\ \phi_i^0=0\ for\ all\ i,\\ u_i^j=U_p,\ \frac{\partial\theta_i^j}{\partial y}=1,\ \frac{\partial\phi_i^j}{\partial y}=1\ \ at\ i=h\\ u_M^j\to U_\infty,\ \theta_M^j\to 0,\ \phi_M^j\to 0\end{array}\right\} \quad (20)$$

Thus the values of *u*, θ and ϕ at grid point *t* = 0 are known; hence the temperature field has been solved at time $t_{i+1}=t_i+\Delta t$ using the known values of the previous time $t=t_i$ for all $i=1, 2, \ldots\ldots, N-1$. Then the velocity field is evaluated using the already known values of temperature and concentration fields obtained at $t_{i+1}=t_i+\Delta t$. These processes are repeated till the required solution of *u*, θ and ϕ is gained at convergence criteria: $abs\left|(u,\ \theta,\ \phi)_{exact}-(u,\ \theta,\ \phi)_{numerical}\right|<10^{-3}$ (21)

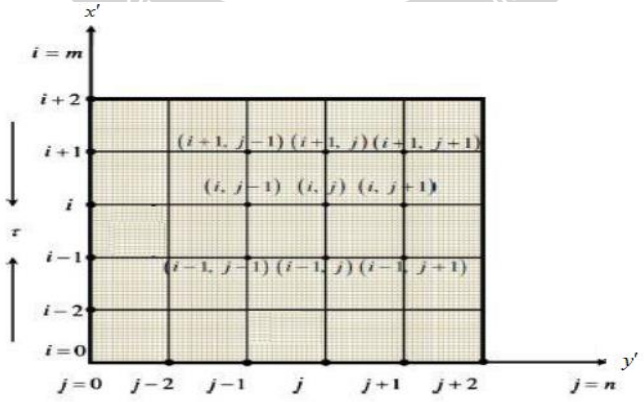

Fig. 2. Finite difference space grid.

IV. PROGRAM CODE VALIDATION

The current finite difference technique has been broadly confirmed in many preceding results and compared with earlier published work in the absence of Rivlin-Ericksen fluid, Angle of inclination and Soret effects. Fig. 3 (Figs. 3(a), 3(b) and 3(c)) demonstrate the evaluation of the velocity, temperature and concentration profiles in comparison with the results of Jagdish Prakash et al. [21]. These three figures show a very good agreement between the results and this lends support to the present numerical code.

 DOI : 10.18231/2454-9150.2018.1296

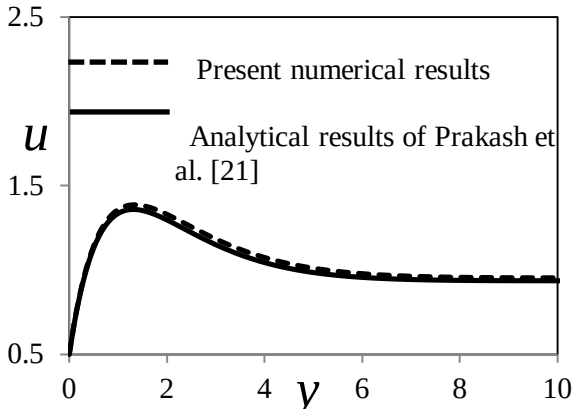

Fig. 3(a).

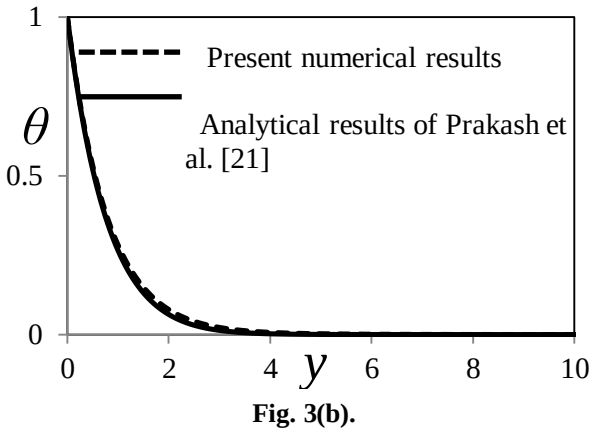

Fig. 3(b).

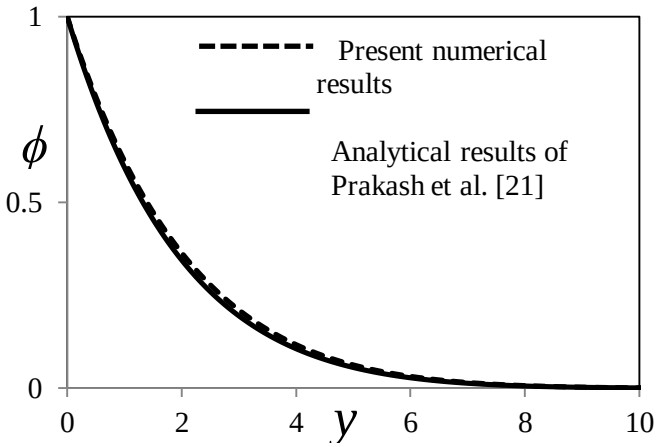

Fig. 3(c).

Fig. 3. Comparison between the boundary layer profiles calculated in the current study and those reported by Previous Results of Jagdish Prakash et al. [21] in absence of Rivlin-Ericksen fluid, Angle of inclination, Soret for different values of Gr = 4.0, Gc = 2.0, Pr = 0.71, R = 1.0, M = 1.0, t = 1.0, Sc = 0.96, A = 0.5, K = 1.0, n = 0.2, Up = 0.5, S = 1.0, Kr = 1.0, ε = 0.02 and Du = 1.0.

V. RESULTS AND DISCUSSIONS

In the previous sections, the problem of unsteady magnetohydrodynamic mixed convection Rivlin-Ericksen fluid flow past an accelerated vertically inclined wavy plate embedded in a porous medium in presence of Soret was formulated and solved by means of a finite element technique, by applying Cogley et al. [44] approximation for the radiative heat flux in energy equation. The expressions for the velocity, temperature, concentration, Skin-friction, Rate of heat and mass transfer coefficients in terms of Nusselt number and Sherwood number were obtained. To illustrate the behaviour of these physical quantities, numerical values were computed with respect to the variations in the governing parameters viz., Hartmann number (M), Permeability parameter (K), Soret number (Sr), Dufour number (Du), Heat absorption parameter (S), Thermal Radiation absorption parameter (R), Rivlin-Ericksen fluid flow parameter (λ), Angle of inclination parameter (α), and Chemical reaction parameter (Kr) separately.

For the physical significance, the numerical discussions in the problem and at t = 1.0, stable values for velocity, temperature and concentration fields are obtained. To find solution of this problem, we have placed an infinite vertical plate in a finite length in the flow. Hence, we solve the entire problem in a finite boundary. However, in the graphs, the y values vary from 0 to 10 and the velocity, temperature and concentration profiles tend to zero as y tend to 10. This is true for any value of y. Thus, we have considered finite length. Throughout the computations, we employ Gr = 2.0, Gc = 2.0, Pr = 0.71, R = 1.0, M = 0.5, t = 1.0, λ = 0.5, $\alpha = \pi/4$, Sc = 0.22, A = 0.5, K = 1.0, n = 0.2, Up = 0.5, S = 1.0, Kr = 1.0, ε = 0.002, Du = 1.0 and Sr = 1.0. From this Fig. 4, different values of Grashof number for heat transfer Gr are chosen from 1.0 to 4.0. The positive value ($Gr > 0$) represents cooling of the plate.

 DOI : 10.18231/2454-9150.2018.1296

The curves in Fig. 4 are plotted to show the influence of Hartmann number M on velocity profiles. It is clear from these curves that velocity decreases when M is increased. Physically, it is justified because the application of transverse magnetic field always results in a resistive type force called Lorentz force which is similar to drag force and tends to resist the fluid motion, finally reducing its velocity. For different values of permeability parameter K shows that velocity is increasing with increasing values of K in Fig. 5. A similar behaviour was expected as the increase in the permeability leads to the increase in the size of the pores inside the porous medium due to which the drag force decreases and velocity increases. For various values of thermal radiation parameter R, the velocity and temperature profile are plotted in Figs. 6. and 7. The thermal radiation parameter R defines the relative contribution of the conduction heat transfer to thermal radiation transfer. It is obvious that an increase in the radiation parameter results in decreasing velocity and temperature within the boundary layer. Figs. 8. and 9 have been plotted to find the variation of velocity and temperature profiles for different values of heat absorption parameter S by fixing other parameters. These figures clearly demonstrates that there is a decrease in velocity and temperature with increase in S. The fact that, when heat is absorbed, the buoyancy force decreases which retards the flow rate and thereby decreases the velocity and temperature profiles, explains this occurrence.

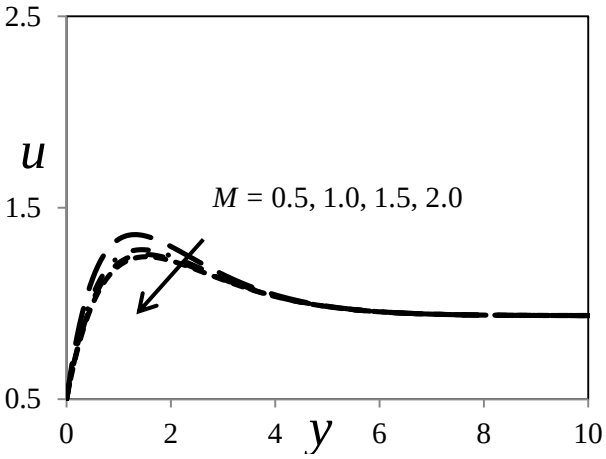

Fig. 4 Influence of *M* on velocity profiles

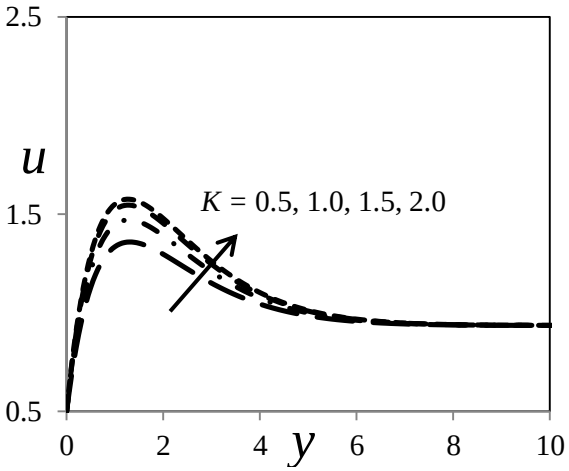

Fig. 5. Influence of *K* on velocity profiles

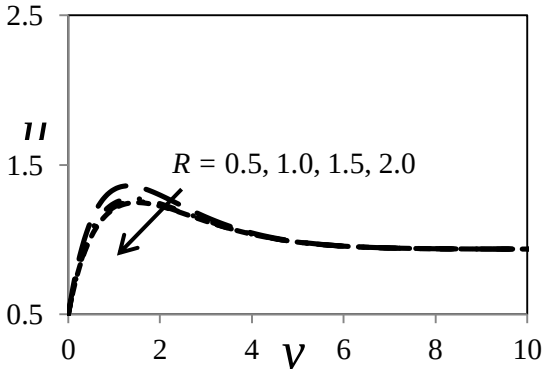

Fig. 6. Influence of *R* on velocity profiles

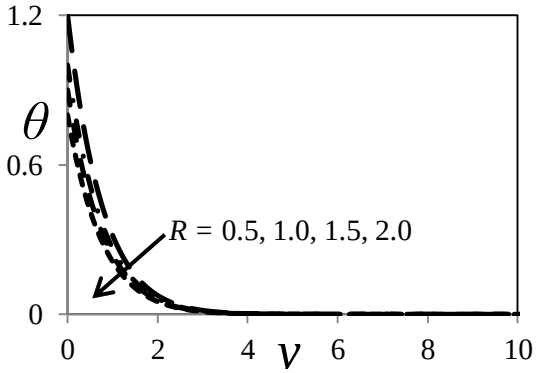

Fig. 7. Influence of *R* on temperature profiles

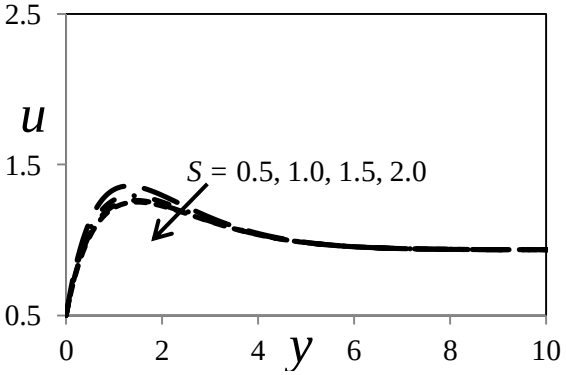

Fig. 8. Influence of *S* on velocity profiles

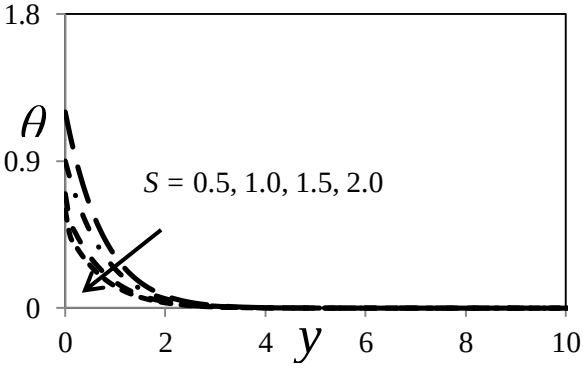

Fig. 9. Influence of *S* on temperature profiles

 DOI : 10.18231/2454-9150.2018.1296

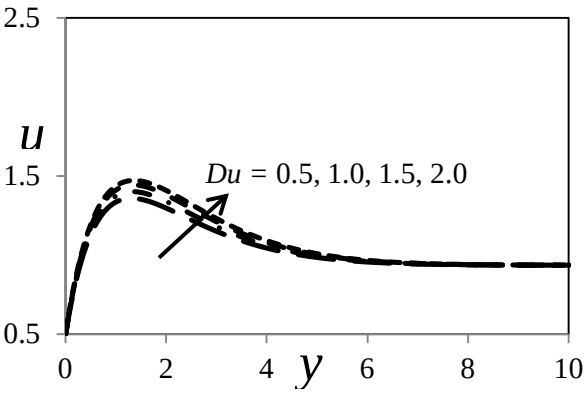

Fig. 10. Influence of *Du* on velocity profiles

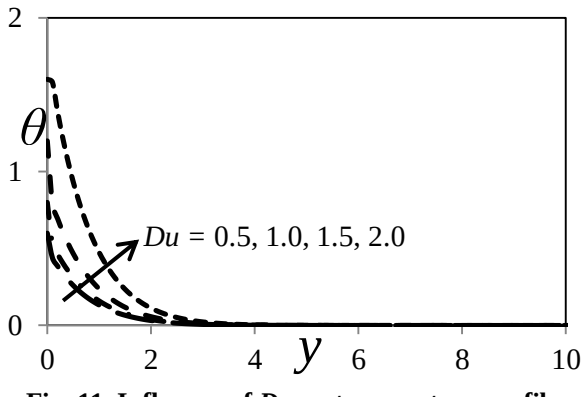

Fig. 11. Influence of *Du* on temperature profiles

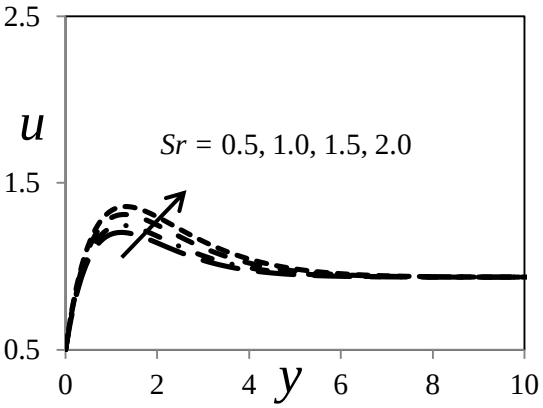

Fig. 12. Influence of *Sr* on velocity profiles

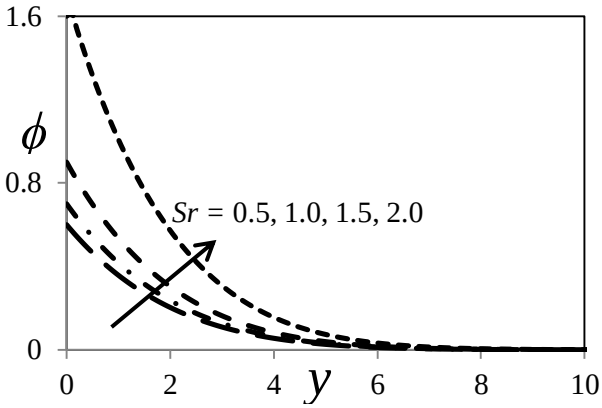

Fig. 13. Influence of *Sr* on concentration profiles

For different values of the Dufour number *Du*, the velocity and temperature profiles are plotted in Figs. 10 and 11. The Dufour number *Du* signifies the contribution of the concentration gradients to the thermal energy flux in the flow. The fact that a growth in the Dufour number causes a rise in the velocity and temperature throughout the boundary layer is observed. The temperature profiles decay smoothly from the plate to the free stream value for *Du*, a well-defined velocity overshoot exists near the plate, and causes the profile to fall to zero at the edge of the boundary layer. Figs. 12 and 13 depict the velocity and concentration profiles for different values of the Soret number *Sr*. The Soret number *Sr* defines the effect of the temperature gradients inducing significant mass diffusion effects. It is noticed that a rise in the Soret number *Sr* results in the augment of the velocity and concentration within the boundary layer.

The influence of Rivlin-Ericksen fluid parameter on velocity profiles is shown in Fig. 14. From this figure, the velocity profiles are decreasing with increasing values of Rivlin-Ericksen fluid parameter. The same effect is observed in Fig. 15 as Angle of inclination increases. Figs. 16 and 17 display the effects of the Chemical reaction parameter *Kr* on the velocity and concentration profiles. As expected, the presence of the chemical reaction influences the concentration profiles as well as the velocity profiles to a large extent. It should be mentioned here that the case study is on a destructive chemical reaction. In fact, as chemical reaction increases, the considerable reduction in the velocity profiles is predicted, and the presence of the peak indicates that the maximum value of the velocity occurs in the body of the fluid close to the surface but not at the surface. Also, a rise in the chemical reaction parameter leads to the reduction in the concentration. It is obvious that the increase in the chemical reaction alters the concentration boundary layer thickness but not the momentum boundary layers.

 DOI : 10.18231/2454-9150.2018.1296

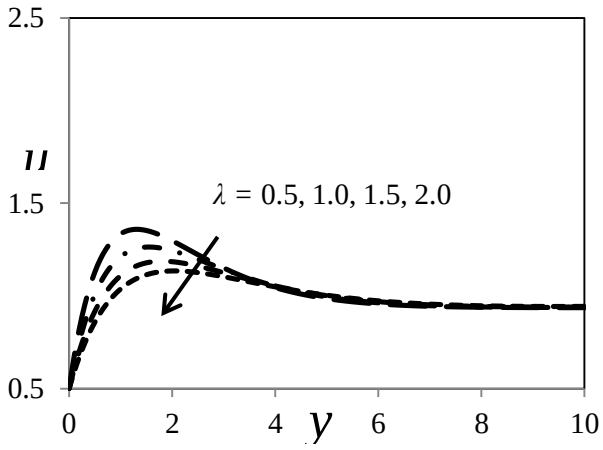

Fig. 14. Influence of λ on velocity profiles

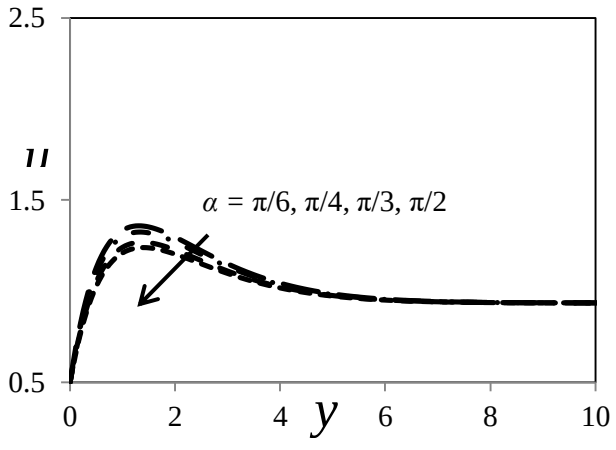

Fig. 15. Influence of α on velocity profiles

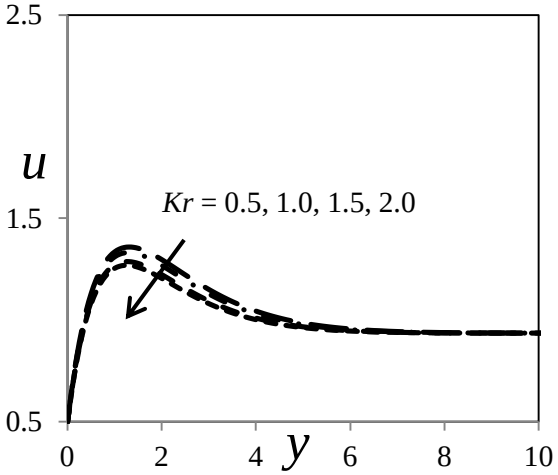

Fig. 16. Influence of *Kr* on velocity profiles

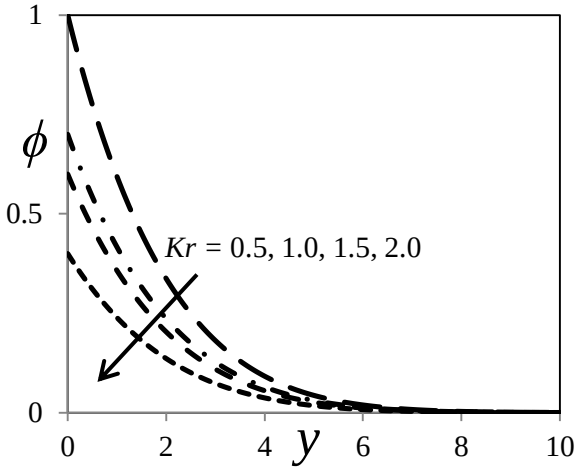

Fig. 17. Influence of *Kr* on concentration profiles

Table-2. Numerical values of Skin-friction coefficient

Gr	*Gc*	*M*	Pr	*Sc*	*K*	*R*	*S*	*Sr*	*Du*	*λ*	*α*	*Kr*	*Up*	*T*	*Cf*
2.0	2.0	0.5	0.71	0.22	0.5	0.5	0.5	0.5	0.5	0.5	π/4	0.5	0.5	1.0	3.152250154
4.0	2.0	0.5	0.71	0.22	0.5	0.5	0.5	0.5	0.5	0.5	π/4	0.5	0.5	1.0	3.415542821
2.0	**4.0**	0.5	0.71	0.22	0.5	0.5	0.5	0.5	0.5	0.5	π/4	0.5	0.5	1.0	3.641158920
2.0	2.0	**1.0**	0.71	0.22	0.5	0.5	0.5	0.5	0.5	0.5	π/4	0.5	0.5	1.0	2.914066058
2.0	2.0	0.5	**7.00**	0.22	0.5	0.5	0.5	0.5	0.5	0.5	π/4	0.5	0.5	1.0	2.952887634
2.0	2.0	0.5	0.71	**0.30**	0.5	0.5	0.5	0.5	0.5	0.5	π/4	0.5	0.5	1.0	2.935423381
2.0	2.0	0.5	0.71	0.22	**1.0**	0.5	0.5	0.5	0.5	0.5	π/4	0.5	0.5	1.0	3.265118339
2.0	2.0	0.5	0.71	0.22	0.5	**1.0**	0.5	0.5	0.5	0.5	π/4	0.5	0.5	1.0	2.987742055
2.0	2.0	0.5	0.71	0.22	0.5	0.5	**1.0**	0.5	0.5	0.5	π/4	0.5	0.5	1.0	2.995333662
2.0	2.0	0.5	0.71	0.22	0.5	0.5	0.5	**1.0**	0.5	0.5	π/4	0.5	0.5	1.0	3.358662847
2.0	2.0	0.5	0.71	0.22	0.5	0.5	0.5	0.5	**1.0**	0.5	π/4	0.5	0.5	1.0	3.402258615
2.0	2.0	0.5	0.71	0.22	0.5	0.5	0.5	0.5	0.5	**1.0**	π/4	0.5	0.5	1.0	3.015528996
2.0	2.0	0.5	0.71	0.22	0.5	0.5	0.5	0.5	0.5	0.5	**π/2**	0.5	0.5	1.0	2.999984125
2.0	2.0	0.5	0.71	0.22	0.5	0.5	0.5	0.5	0.5	0.5	π/4	**1.0**	0.5	1.0	2.984462186
2.0	2.0	0.5	0.71	0.22	0.5	0.5	0.5	0.5	0.5	0.5	π/4	0.5	**1.0**	1.0	3.201586295
2.0	2.0	0.5	0.71	0.22	0.5	0.5	0.5	0.5	0.5	0.5	π/4	0.5	0.5	**2.0**	3.162599868

The effects of thermal Grashof number (*Gr*), solutal Grashof number (*Gc*), Prandtl number (Pr), Schmidt number (*Sc*), Hartmann number (*M*), Permeability parameter (*K*), Soret number (*Sr*), Dufour number (*Du*), Heat absorption parameter (*S*), Thermal Radiation absorption parameter (*R*), Rivlin-Ericksen fluid flow parameter (λ)), Angle of inclination parameter (α), Plate velocity (U_p), time (t) and Chemical reaction parameter (*Kr*) on skin-friction coefficient is presented in table 2 with the help of numerical values. From this table, it is observed that, the numerical values of skin-friction coefficient is increasing under the increasing of thermal Grashof number (*Gr*), solutal Grashof number (*Gc*), Permeability parameter (*K*), Soret number (*Sr*), Dufour number (*Du*), Plate velocity (U_p) and time (t), while it decreasing under the increasing of Prandtl number (Pr),

 DOI : 10.18231/2454-9150.2018.1296

Schmidt number (*Sc*), Hartmann number (*M*), Heat absorption parameter (*S*), Thermal Radiation absorption parameter (*R*), Rivlin-Ericksen fluid flow parameter (λ), Angle of inclination parameter (α) and Chemical reaction parameter (*Kr*).

The effects Prandtl number (Pr), Dufour number (*Du*), Heat absorption parameter (*S*), Thermal Radiation absorption parameter (*R*) and time (*t*) on rate of heat transfer coefficient in terms of Nusselt number is discussed in table 3. From this table, it is observed that, the numerical values of Nusselt number coefficient is increasing with the increasing of Dufour number (*Du*) and time (*t*) and the reverse effect is observed with the increasing values of Prandtl number (Pr), Heat absorption parameter (*S*) and Thermal Radiation absorption parameter (*R*). Table 4, shows the numerical values of rate of mass transfer coefficient in terms of Sherwood number coefficient for different values of Schmidt number (*Sc*), Soret number (*Sr*), time (*t*) and Chemical reaction parameter (*Kr*). From this table, it is observed that Sherwood number coefficient is increasing with increasing values of Soret number (*Du*) and time (*t*) and decreasing with increasing of Schmidt number (*Sc*) and Chemical reaction parameter (*Kr*).

Table-3. Numerical values of Nusselt number coefficient

Pr	*R*	*S*	*Du*	*t*	*Nu*
0.71	0.5	0.5	0.5	1.0	0.985521475
7.00	0.5	0.5	0.5	1.0	0.621589963
0.71	**1.0**	0.5	0.5	1.0	0.758841203
0.71	0.5	**1.0**	0.5	1.0	0.810215569
0.71	0.5	0.5	**1.0**	1.0	1.089952617
0.71	0.5	0.5	0.5	**2.0**	1.065548269

Table-4. Numerical values of Sherwood number coefficient

Sc	*Kr*	*Sr*	*t*	*Sh*
0.22	0.5	0.5	1.0	0.901154862
0.30	0.5	0.5	1.0	0.784152633
0.22	**1.0**	0.5	1.0	0.801542366
0.22	0.5	**1.0**	1.0	1.056624891
0.22	0.5	0.5	**2.0**	0.941156231

VI. CONCLUSIONS

The numerical investigation has been carried out in the present study to analyze the influence of governing over a vertically inclined plate embedded in a porous medium in the presence of non-uniform heat source, thermal diffusion, diffusion thermo, thermal radition and first order chemical reaction. The governing non-linear partial differential equations are formulated into linear partial differential equations with the help of non-dimensional variables. And being solved numerically by using finite difference method. We have acquired interesting observations graphically for these pertinent parameters which are summarized below:

1. Velocity increases with an increase in *Sr*, *Du*, *K* where as it decreases with increasing of λ, α, *S* and *R*.
2. *M* retards the velocity of the flow field at all points, due to the magnetic pull of the Lorentz force acting on the flow field.
3. The fluid motion is retarded due to *Kr*. Hence the consumption of chemical species causes a fall in the concentration field which in turn diminishes the buoyancy effects due to concentration gradients.
4. The rate of heat transfer or Nusselt number coefficient increases with increasing of *Du* where as it shows reverse effect in the case of *R* and *S*.
5. The rate of mass transfer coefficient or Sherwood number decreases with an increase in *Sc* and *Kr*.
6. This study exactly agrees with the finding of previous results of Jagdish Prakash et al. [21] in absence of λ, α and *Sr*.

REFERENCES

[1] R. Seigel, J. R. Howell, Thermal radiation heat transfer, student ed., Macgraw-Hill (1971).

[2] K. Srihari, G. Srinivas Reddy, Effects of radiation and Soret in the presence of heat source/sink on unsteady MHD flow past a semi-infinite vertical plate, Brit J Math Comput Sci (4) (2014), pp. 2536-2556.

[3] A. K. Waqar, H. K. Zafar, O.D. Makinde, Non-aligned MHD stagnation point flow of variable viscosity nanofluids past a stretching sheet with radiative heat, Int J Heat Mass Transfer, 96 (2016), pp. 525-534.

[4] O. D. Makinde, A. K. Waqar, C. J. Richard, MHD variable viscosity reacting flow over a convectively heated plate in a porous medium with thermophoresis and radiative heat transfer, Int J Heat Mass Transfer, 93 (2016), pp. 595-604.

[5] A. E. Magdy, Free convection effects on perfectly conducting fluid, Int J Eng Sci, 39 (7) (2001), pp. 799-819.

[6] D. Pal, G. Mandal, Hydromagnetic convective-radiative boundary layer flow of nanofluids induced by a non-linear vertical stretching/shrinking sheet with viscous-Ohmic dissipation, Powder Tech, 279 (2015), pp. 61-74.

[7] Y. Lin, B. Li, L. Zheng, G. Chen, Particle shape and radiation effects on Marangoni boundary layer flow and heat transfer of copper-water nanofluid driven by an exponential temperature, Powder Tech, 301 (2016), pp. 379-386.

[8] M. Sheikholeslami, T. Hayat, A. Alsaedi, MHD free convection of Al2O3-water nanofluid considering thermal radiation: a numerical study, Int J Heat Mass Transfer, 96 (2016), pp. 513-524.

[9] S. A. Shehzad, Z. Abdullah, A. Alsaedi, F. M. Abbasi, T. Hayat, Thermally radiative three-dimensional flow of Jeffrey nanofluid with internal heat generation and magnetic field, J Magnet Magn Mater, 397 (2016), pp. 108-114.

[10] F. S. Ibrahim, M. A. Mansour, M. A. A. Hamad, Lie-group analysis of radiative and magnetic field effects on free

 DOI : 10.18231/2454-9150.2018.1296

convection and mass transfer flow past a semi-infinite vertical flat plate, Electron J Differ Eq, 39 (2005), pp. 1-17.

[11] M. A. Mansur, Radiation and free-convection effect on the oscillatory flow past a vertical plate, NASA astrophysics data system, Kluwer Academic Publishers (1989), pp. 269-275.

[12] S. S. Ghadikolaei, Kh. Hoseinzadeh, M. Yassari, H. Sadeghi, D. D. Ganji, Boundary layer of micropolar dusty fluid with TiO_2 nanoparticles in a porous medium under the effect of magnetic field and thermal radiation over a stretching sheet, J. Mol. Liq., 244 (2017), pp. 374-389.

[13] B. Mahanthesh, B. J. Gireesha, R. S. Reddy Gorla, F. M. Abbasi, S. A. Shehzad, Numerical solutions for magnetohydrodynamic flow of nanofluid over a bidirectional non-linear stretching surface with prescribed surface heat flux boundary, J. Magn. Magn. Mater., 417 (2016), pp. 189-196.

[14] B. Mahanthesh, B. J. Gireesha, Rama S. R. Gorla, O. D. Makinde, Magnetohydrodynamic three-dimensional flow of nanofluids with slip and thermal radiation over a nonlinear stretching sheet: a numerical study, Neural Comput. Appl. (2016), pp. 1-11.

[15] M. A. Hossain, M. A. Alim, D. A. S. Rees, The effect of radiation on free convection from a porous vertical plate, Int. J. Heat Mass Transf., 42 (1) (1998), pp. 181-191.

[16] D. Srinivasacharya, Upendar Mendu, Free convection in MHD micro polar fluid with radiation and chemical reaction effects, Chem. Ind. Chem. Eng. Q., 20 (2) (2014), pp. 183-195.

[17] D. Srinivasacharya, Ch. RamReddy, Natural convection heat and mass transfer in a micro polar fluid with thermal and mass stratification, Int. J. Comp. Meth. Eng. Sci. Mech., 14 (2013), pp. 401-413.

[18] M. A. Seddeek, A. A. Darwish, M. S. Abdelmeguid, Effects of chemical reaction and variable viscosity on hydromagnetic mixed convection heat and mass transfer for Hiemenz flow through porous media with radiation, Commun. Nonlinear Sci. Numer. Simul., 12 (2) (2007), pp. 195-213.

[19] F. S. Ibrahim, A. M. Elaiw, A. A. Bakr, Effect of the chemical reaction and radiation absorption on the unsteady MHD free convection flow past a semi infinite vertical permeable moving plate with heat source and suction, Commun. Nonlinear Sci. Numer. Simul., 13 (6) (2008), pp. 1056-1066.

[20] O. D. Makinde, P. O. Olanrewaju, W. M. Charles, Unsteady convection with chemical reaction and radiative heat transfer past a flat porous plate moving through a binary mixture, Afrika Matematika, 21 (1) (2011), pp. 1-17.

[21] Jagdish Prakash, Bangalore Rushi Kumar, and Ramachandran Sivaraj, Radiation and Dufour effects on unsteady MHD mixed convective flow in an accelerated vertical wavy plate with varying temperature and mass diffusion, Walailak J. Sci. Technol., vol. 11, pp. 939-954, 2014.

[22] K. Vajravelu, A. Hadjinicolaou, Convective heat transfer in an electrically conducting fluid at a stretching surface with uniform free stream, Int J Eng Sci, 35 (1997), p. 1237.

[23] Cogley, A.C., Vincenti, W.G., and Gill, S.E., Differential approximation for radiative transfer in a non-gray-gas near equilibrium, AIAA J., vol. 6, pp. 551-553, 1968.

 DOI : 10.18231/2454-9150.2018.1296